2012

Functional and structural studies of the disulfide isomerase DsbC from the plant pathogen Xylella fastidiosa reveals a redox-dependent oligomeric modulation in vitro

FEBS JOURNAL, HOBOKEN, v. 279, n. 20, supl. 1, Part 3, pp. 3828-3843, OCT, 2012
http://www.producao.usp.br/handle/BDPI/32593

the FEBS Journal

Functional and structural studies of the disulfide isomerase DsbC from the plant pathogen *Xylella fastidiosa* reveals a redox-dependent oligomeric modulation *in vitro*

Clelton A. Santos[1], Marcelo A. S. Toledo[1], Daniela B. B. Trivella[2], Lilian L. Beloti[1], Dilaine R. S. Schneider[1], Antonio M. Saraiva[1], Aline Crucello[1], Adriano R. Azzoni[1,3], Alessandra A. Souza[4], Ricardo Aparicio[2] and Anete P. Souza[1,5]

1 Centro de Biologia Molecular e Engenharia Genética, Universidade Estadual de Campinas, Brazil
2 Laboratório de Biologia Estrutural e Cristalografia, Instituto de Química, Universidade Estadual de Campinas, Brazil
3 Departamento de Engenharia Química, Escola Politécnica, Universidade de São Paulo, Brazil
4 Centro APTA Citros Sylvio Moreira/IAC, Cordeirópolis, Brazil
5 Departamento de Biologia Vegetal, Instituto de Biologia, Universidade Estadual de Campinas, Brazil

Keywords
biofilm formation; DsbC; oligomeric assembly; SAXS; *Xylella fastidiosa*

Correspondence
A. P. Souza, Centro de Biologia Molecular e Engenharia Genética (CBMEG), Universidade Estadual de Campinas, Rua Candido Rondon 400, Cidade Universitária 'Zeferino Vaz', CP 6010, 13083-875, Campinas, São Paulo, Brazil
Fax: +55 19 3521 1089
Tel: +55 19 3521 1089
E-mail: anete@unicamp.br

(Received 23 May 2012, revised 1 August 2012, accepted 6 August 2012)

doi:10.1111/j.1742-4658.2012.08743.x

Xylella fastidiosa is a Gram-negative bacterium that grows as a biofilm inside the xylem vessels of susceptible plants and causes several economically relevant crop diseases. In the present study, we report the functional and low-resolution structural characterization of the *X. fastidiosa* disulfide isomerase DsbC (XfDsbC). DsbC is part of the disulfide bond reduction/isomerization pathway in the bacterial periplasm and plays an important role in oxidative protein folding. In the present study, we demonstrate the presence of XfDsbC during different stages of *X. fastidiosa* biofilm development. XfDsbC was not detected during *X. fastidiosa* planktonic growth; however, after administering a sublethal copper shock, we observed an overexpression of XfDsbC that also occurred during planktonic growth. These results suggest that *X. fastidiosa* can use XfDsbC *in vivo* under oxidative stress conditions similar to those induced by copper. In addition, using dynamic light scattering and small-angle X-ray scattering, we observed that the oligomeric state of XfDsbC *in vitro* may be dependent on the redox environment. Under reducing conditions, XfDsbC is present as a dimer, whereas a putative tetrameric form was observed under nonreducing conditions. Taken together, our findings demonstrate the overexpression of XfDsbC during biofilm formation and provide the first structural model of a bacterial disulfide isomerase in solution.

Structured digital abstract

- **XfDsbC** and **XfDsbC** bind by x ray scattering (View Interaction: 1, 2)
- **XfDsbC** and **XfDsbC** bind by molecular sieving (View interaction)
- **XfDsbC** and **XfDsbC** bind by comigration in non denaturing gel electrophoresis (View interaction)
- **XfDsbC** and **XfDsbC** bind by cross-linking study (View Interaction: 1, 2)
- **XfDsbC** and **XfDsbC** bind by dynamic light scattering (View Interaction: 1, 2)

Abbreviations

DLS, dynamic light scattering; EcDsbC, *Escherichia coli* DsbC; HiDsbC, *Haemophilus influenzae* DsbC; PDB, Protein Data Bank; Rg, radius of gyration; SAXS, small-angle X-ray scattering; TCEP, *tris*(2-carboxyethyl)phosphine; XcDsbC, *Xanthomonas campestris* DsbC; XfDsbC, *Xylella fastidiosa* disulfide isomerase DsbC; $XfDsbC_{N\text{-}Red}$, nonreduced XfDsbC; $XfDsbC_{Red}$, reduced XfDsbC.

Introduction

Disulfide bond formation is a critical step for the correct folding of many proteins that are rich in cysteine residues. In addition to conferring a stable structure, disulfide bonds play a regulatory role by changing the shape, surface charge or reactivity of some proteins [1]. Among the Gram-negative bacteria, the Dsb protein family constitutes the oxidative protein folding machinery and plays an important role in disulfide bond formation in the periplasm [2–5]. The enzymatic pathway of the Dsb protein family is well characterized in *Escherichia coli* and is composed of five members: DsbA, DsbB, DsbC, DsbD and DsbG [5]. These proteins are typically oxidoreductases and contain a CXXC motif (cysteine residues separated by two amino acids) in the catalytic site, similar to thioredoxin-like proteins [6].

Chemically, DsbA, which is a strong thiol oxidant, catalyzes disulfide bond formation [7,8]. DsbA rapidly oxidizes cysteine residues in proteins that are located in the periplasm by introducing a disulfide bond that is more energetically favourable for correct protein folding [9]. However, two cysteines can be incorrectly joined in a disulfide bond that does not appear in the native protein conformation. When mis-oxidized, the non-native disulfide bond may be reduced or rearranged to ensure that correct protein folding is achieved. DsbC catalyzes this step in the reduction/isomerization pathway [4,10,11].

Two models have been proposed to explain how *E. coli* DsbC (EcDsbC) reshuffles proteins containing incorrect disulfide bonds [5]. However, the biological role of DsbC in other bacteria is not completely understood. In addition to isomerase activity, DsbC exhibits certain chaperone-like properties [12], and this function appears to be independent of the two cysteines in the active site CXXC motif [13]. The isomerase and chaperone activities of DsbC are important for bacterial pathogenicity because these activities ensure the correct folding in a wide range of proteins, including secreted virulence factors and surface components such as adhesins and pili [14].

An interesting aspect of the disulfide bond isomerization mechanism is that the active-site cysteine residues must remain reduced for DsbC activity. This characteristic is particularly intriguing because DsbC acts in the bacterial periplasm, which is an oxidizing environment. DsbD, a transmembrane protein that transfers reducing equivalents from the cytosol to the periplasm, is responsible for maintaining DsbC in the reduced and active state [10,15].

Interestingly, a study of eukaryotic protein disulfide isomerase, which is topologically analogous to prokaryotic DsbC, revealed an intramolecular structural rearrangement between the catalytic and noncatalytic domains that was dependent on the environmental redox state [16]. Protein disulfide isomerase is composed of two catalytic domains (a and a′) that are separated by two noncatalytic domains (b and b′) and a third domain (c) [17]. Correspondingly, EcDsbC is described as a V-shaped homodimeric protein in which each monomer contains an N-terminal dimerization domain that is joined by a hinged linker to the C-terminal catalytic domain [18].

In *E. coli* mutants lacking *dsbC*, many cysteine-rich proteins exhibited reduced activity or were degraded [11,19,20]. However, the most expressive phenotype observed in *dsbC*-null mutants is an increased sensitivity to copper (a redox-active metal), which indicates that DsbC is required for the oxidative stress response [21].

In the present study, we report the functional and structural characterization of DsbC from the 9a5c strain of *Xylella fastidiosa* (XfDsbC) by small-angle X-ray scattering (SAXS). *X. fastidiosa* is a Gram-negative bacterium that grows as a biofilm in the xylem vessels of susceptible plants and causes many diseases in commercial crops around the world, including citrus variegated chlorosis, an economically important crop disease that compromises sweet orange production in Brazil [22,23]. We characterized XfDsbC to evaluate its role in biofilm formation, which blocks the xylem and causes the onset of disease. The results obtained demonstrate that XfDsbC expression occurs during bacterial biofilm formation and is enhanced under oxidative stress conditions. In addition, using modelling approaches based on the SAXS data, we provide evidence for a possible redox-dependent oligomeric modulation of XfDsbC *in vitro*.

Results

XfDsbC is involved in biofilm formation and the copper stress response

We investigated the involvement of XfDsbC in *X. fastidiosa* biofilm formation and development. XfDsbC was successfully cloned, and the protein was purified by affinity chromatography. XfDsbC has a molecular mass of 29.5 kDa, which corresponds to the 263-amino acid sequence encoded by ORF *Xf*1177 plus the C-terminal His_6-Tag added by the pET29a(+) vector. Titration of the number of free cysteines revealed that the recombinant XfDsbC was purified in an oxidized

state as reported previously [24]. Polyclonal antibodies against XfDsbC were produced and used for western blot analysis. We observed a differential expression pattern of XfDsbC during *X. fastidiosa* biofilm formation and planktonic cell growth (Fig. 1). XfDsbC was expressed during all phases of biofilm development. However, during the planktonic growth phase of *X. fastidiosa*, XfDsbC was poorly expressed and could not be detected by western blotting (Fig. 1A). However, after administering a sublethal copper shock, the planktonic cells overexpressed XfDsbC (Fig. 1B). The samples were normalized against total protein concentration before gel loading to ensure that the same amount of protein was evaluated for each condition. These results suggest that *X. fastidiosa* can use XfDsbC *in vivo* under oxidative stress conditions similar to those induced by copper. The statistical analysis of the ratio of the intensity and area (pixels) of the bands visualized on nitrocellulose membranes revealed statistically significant differences ($P < 0.05$) in the expression profiles of XfDsbC (Fig. 1C, D). Under copper-induced oxidative stress, the expression of XfDsbC was only significantly greater in biofilms than in planktonic cells after 5, 10 and 30 days of biofilm growth (Fig. 1D). The intensities of the protein bands corresponding to XfDsbC in the different phases of biofilm formation in the presence or absence of copper stress were similar to the profiles observed for planktonic cells and biofilms exposed to copper shock. At 15 and 20 days, there were no significant differences ($P < 0.05$) in XfDsbC expression between biofilms in the presence or absence of copper. However, at 3 and 5 days, XfDsbC was expressed in larger quantities in the biofilms that were not treated with copper, whereas, at 10 and 30 days, XfDsbC was expressed in larger quantities in the biofilm cells that were subjected to copper stress (Fig. 1C, D).

XfDsbC expression complements the *dsbC*-defective *E. coli* mutant

The thiol-disulfide reductase activity of purified nonreduced XfDsbC ($XfDsbC_{N\text{-}Red}$) was confirmed *in vitro* using the rate of insulin disulfide reduction (Fig. 2A). As expected, the activity of XfDsbC was comparable to that of EcDsbC. The insulin reduction rate of XfDsbC was 0.0126 ($\Delta A_{650}{\cdot}min^{-2}$), which was approximately 88% of the activity of EcDsbC [0.0143 ($\Delta A_{650}{\cdot}min^{-2}$)]. In addition to the reductase activity, the disulfide bond isomerase activity of XfDsbC was assessed *in vivo* in a *dsbC E. coli* mutant. This *dsbC*-defective *E. coli* mutant was used because an appropriate methodology for the construction of the *X. fastidiosa* 9a5c mutants is not yet available. DsbC isomerase activity is required for

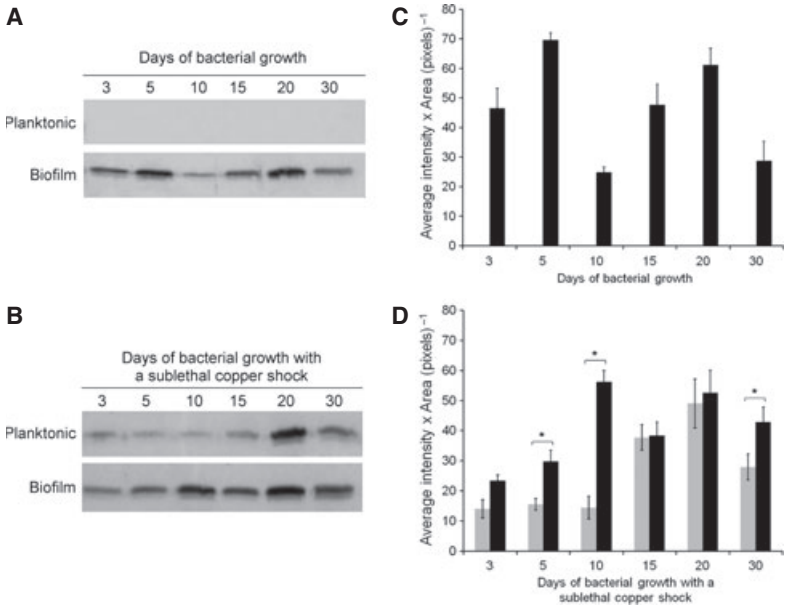

Fig. 1. XfDsbC expression in *X. fastidiosa* is elevated during biofilm formation and the oxidative stress response. Total protein samples were isolated from different biofilm growth phases and planktonic cells (see Experimental procedures), normalized using BCA quantification, and evaluated by western blot analysis using polyclonal antibodies against XfDsbC in the absence (A) or presence (B) of oxidative stress induced by copper. (C) The XfDsbC expression profiles of biofilm (black bars) and planktonic (grey bars) cells in the absence or (D) presence of copper were quantified using EDAS software. The bars represent the mean of three independent experiments. The error bars indicate the SE obtained from triplicate experiments. Asterisks indicate statistically significant differences ($P < 0.05$, *t*-test).

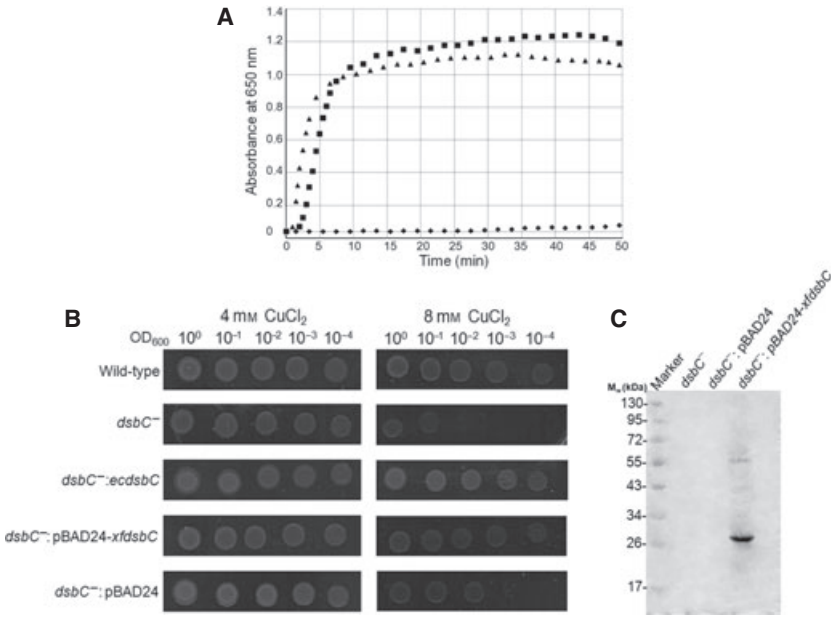

Fig. 2. XfDsbC functionally complements a *dsbC*-null *E. coli* mutant. (A) The $XfDsbC_{N\text{-}Red}$ (▲) thiol-reductase activity was confirmed *in vitro* using the insulin disulfide reduction assay. EcDsbC (■) and a test without catalyst (♦) were used as positive and negative controls, respectively. (B) The XfDsbC disulfide bond isomerase activity was assessed *in vivo* for its ability to complement an *E. coli* mutant lacking *dsbC* (*dsbC*$^-$). The *dsbC* phenotypes of the various strains (wild-type, *dsbC*$^-$, *dsbC*$^-$ containing pBAD24-*xfdsbC*, and *dsbC*$^-$ with a wild-type *ecdsbC* gene or empty vector) were evaluated by spotting 5 μL of 10-fold serial dilutions onto BHI agar plates with the appropriate antibiotic and containing 4 or 8 mM $CuCl_2$ with 0.002% (w/v) L-arabinose. The plates were incubated overnight at 37 °C, and the ability of XfDsbC to restore the wild-type phenotype was analyzed. (C) The expression of XfDbsC in the *dsbC*$^-$ strain was confirmed by western blot analysis.

tolerance to copper, a redox-active metal [21]. Copper is a nonspecific thiol oxidant that leads to protein misfolding through the establishment of non-native disulfide bonds. The DsbC reduction/isomerization pathway acts to reverse protein misfolding by rearranging the disulfide bonds and promoting native protein folding. XfDsbC expression complemented the *dsbC*$^-$ *E. coli* mutant under the oxidative stress conditions induced by copper (i.e. the transformation of the *dsbC*$^-$ mutant strain with pBAD24-*xfdsbC* restored the wild-type phenotype) (Fig. 2B). In addition, western analysis of XfDsbC in *dsbC*$^-$ cells containing pBAD24-*xfdsbC* that were grown on plates containing 8 mM $CuCl_2$ (Fig. 2C) strongly suggests that the increased cell viability under this condition is correlated with the presence of XfDsbC. Our findings show that the basal expression of *xfdsbC* can support the growth of the *dsbC*$^-$ *E. coli* mutant strain even in the absence of L-arabinose, which induces the arabinose operon in the pBAD24 vector (data not shown).

Initial characterization of XfDsbC

The initial analysis of the amino acid sequence of XfDsbC revealed the presence of 21 N-terminal amino acid residues that are not present in the homologous EcDsbC and *Erwinia chrysanthemi* proteins (Fig. S1). Interestingly, these additional N-terminal amino acids are also found in the bacterium *Xanthomonas campestris* DsbC (XcDsbC), which has host specificity for the same citrus plants infected by *X. fastidiosa*. Four cysteine residues similar to those observed in the 3D structure of EcDsbC [18] are present in the thioredoxin-like domains of XfDsbC. The Cys143 and Cys146 residues of XfDsbC (active site) correspond to Cys98 and Cys101 of the EcDsbC crystal structure [Protein Data Bank (PDB) code: 1EEJ], and the Cys186 and Cys208 residues of XfDsbC (non-active site) correspond to Cys141 and Cys163 of EcDsbC. These cysteine residues are strongly conserved between DsbC homologues and, because DsbC can undergo structural changes that are dependent on the redox environment, these cysteine residues may be directly or indirectly involved in structural rearrangements and function. Therefore, we evaluated whether the redox environment caused changes in the structure of XfDsbC *in vitro*. XfDsbC samples in the presence or absence of reducing agents were analyzed using SDS/PAGE, native gel electrophoresis, CD, size-exclusion chromatography, fluorimetry, chemical cross-linking and dynamic light scattering (DLS).

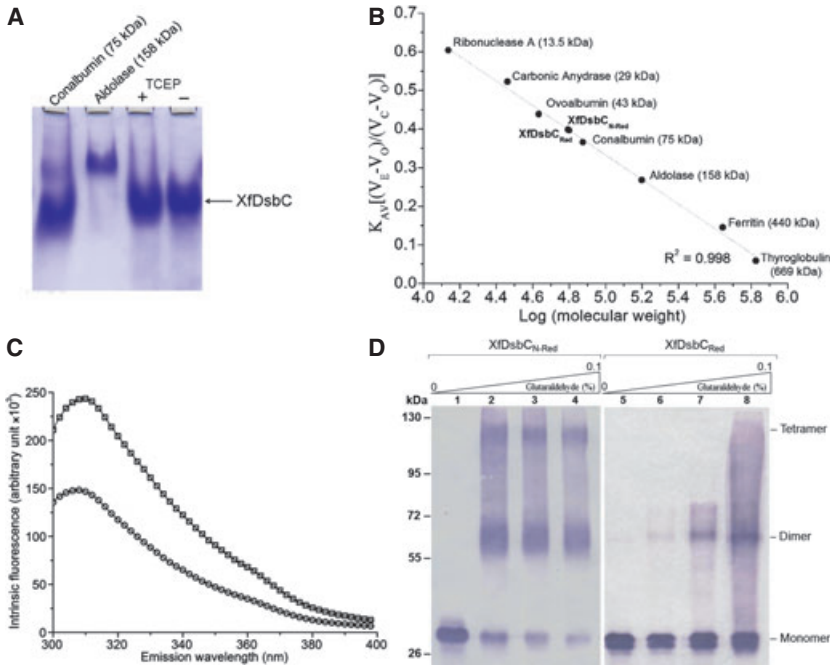

Fig. 3. Initial characterization of XfDsbC. (A) XfDsbC nondenaturing polyacrylamide gel electrophoresis in the presence (+) and absence (–) of TCEP. (B) Size-exclusion chromatography calibration curves for $XfDsbC_{Red}$ and $XfDsbC_{N\text{-}Red}$. The monomeric molecular mass for XfDsbC is 29.5 kDa, and the expected molecular mass for the XfDsbC dimer is 59 kDa. The estimated molecular masses for $XfDsbC_{Red}$ and $XfDsbC_{N\text{-}Red}$ were 60.2 and 61.7 kDa, respectively. (C) XfDsbC fluorimetry spectra of $XfDsbC_{Red}$ and $XfDsbC_{N\text{-}Red}$ are shown as squares and circles, respectively. (D) Glutaraldehyde cross-linking of XfDsbC in the absence ($XfDsbC_{N\text{-}Red}$) and presence ($XfDsbC_{Red}$) of TCEP. The XfDsbC samples (5 μM) were treated with increasing concentrations of glutaraldehyde (0%, 0.025%, 0.05% and 0.1%), and the products were evaluated by western blot analysis using polyclonal antibodies against XfDsbC.

Under denaturing conditions in the presence and absence of β-mercaptoethanol, XfDsbC was present in the gel as a single band at approximately 29 kDa, which corresponds to the molecular mass of the monomer. Under nondenaturing conditions, XfDsbC samples exhibited the same gel migration profile in the presence and absence of *tris*(2-carboxyethyl)phosphine (TCEP). This profile was more similar to that of conalbumin (75 kDa) than that of aldolase (158 kDa) (Fig. 3A). The CD analysis revealed a typical protein spectrum with a predominantly α-helical structure (38% helical/18% sheet), similar to that for EcDsbC calculated from its crystal structure [18]. There were no significant differences in the secondary structure content of XfDsbC in the presence or absence of TCEP (data not shown).

Analytical size-exclusion chromatography of reduced and nonreduced XfDsbC confirmed the native gel results, indicating that there were no differences between the two tested conditions (Fig. 3B). Both the reduced and nonreduced protein samples eluted as single peaks in the gel filtration assays, with retention times that corresponded to apparent molecular masses of 60.2 and 61.7 kDa, respectively (Fig. 3B). Different buffer and pH conditions, as well as XfDsbC oxidation under atmospheric oxygen, were evaluated, and no differences were observed in the elution profiles of the samples in the presence or absence of the reducing agent (data not shown).

The conformational changes in the XfDsbC protein samples under reducing or nonreducing conditions were next analyzed by fluorimetry, and tryptophan emission was used as a probe to monitor DsbC folding. XfDsbC contains a tryptophan residue that neighbours Cys186, which is distal from the active site (Fig. S1). This cysteine residue can establish a disulfide bond with Cys208 and likely plays a role in XfDsbC folding. The fluorescence spectra recorded upon excitation at 280 nm showed that reduction with TCEP increased the intrinsic fluorescence intensity and shifted the maximum emission wavelength from 307 to 310 nm (Fig. 3C).

Although XfDsbC can exist predominantly as dimers in solution, and SDS/PAGE, nondenaturing gel electrophoresis, CD and size-exclusion chromatography did not reveal any redox-dependent structural

changes in XfDsbC, higher-order oligomeric species that appear to correspond to tetramers were observed *in vitro* under the nonreduced condition of XfDsbC (Fig. 3D, lanes 1–4) after chemical cross-linking with glutaraldehyde, along with dimeric and monomeric species (Fig. 3D, lanes 2–4). However, only dimeric forms, in addition to monomeric species, were observed under the reduced condition (Fig. 3D, lanes 5–8). These slow-migrating species were not observed in the absence of glutaraldehyde (Fig. 3D, lanes 1 and 5).

We also used DLS analysis to assess the redox-dependent oligomeric modulation of XfDsbC. The results of this analysis showed that, under both nonreduced and reduced conditions, XfDsbC showed a low index of polydispersity (%Pd; 9.5 and 5.8, respectively) (Table 1). In addition, the molecule in solution under the nonreduced condition presents a hydrodynamic diameter (D_h) of 4.6 nm and differs from that observed under the reduced condition which has a D_h of 3.8 nm, indicating of the presence of a high oligomer form of XfDsbC under the nonreduced condition.

SAXS analysis suggests a redox-dependent oligomeric assembly of XfDsbC *in vitro*

XfDsbC SAXS scattering curves collected in the presence and absence of reducing agent were analyzed. The scattering curves of 4- and 7-mg·mL^{-1} protein samples in the presence of 3 mM TCEP [reduced XfDsbC ($XfDsbC_{Red}$)] were collected. The 7-mg·mL^{-1} samples exhibited interparticle interference effects that compromised further analysis, although the curves collected from 4-mg·mL^{-1} samples did not exhibit this behaviour. Therefore, the scattering curves of XfDsbC at 4 mg·mL^{-1} were selected for SAXS data analyses and model construction. The superimposition of the 20 scattering curves collected for $XfDsbC_{Red}$ at 4 mg·mL^{-1} revealed a transition during the data collection that may be the result of conformational changes arising from radiation damage. Therefore, only the first curve was used for further analysis (Fig. 4A). As shown in Fig. 4A (inset), the constructed $XfDsbC_{Red}$ Guinier plot demonstrated a linear behaviour, indicating sample monodispersity. The Guinier analysis revealed a radius of gyration (Rg) of 31.2 Å. $XfDsbC_{Red}$ Kratky plots were also constructed (Fig. 4B) and displayed a well-defined maximum, which is expected for the native state of a compact globular protein. The molecular mass of the scattering particles was estimated to be 66 kDa by SAXS MOW software [25]. This suggests that $XfDsbC_{Red}$ is a dimer in solution, similar to other DsbC proteins [18,26]. The $XfDsbC_{Red}$ distance distribution function, $P(r)$, showed a maximum intramolecular distance (D_{max}) of 100 Å (Fig. 4D). The Rg calculated from the $P(r)$ was 31.5 Å, which is consistent with the values obtained from the Guinier analysis.

Scattering curves were collected from 1, 4 and 13 mg·mL^{-1} XfDsbC in the absence of TCEP ($XfDsbC_{N\text{-}Red}$). However, the curves at 1 mg·mL^{-1} were too dilute for SAXS data collection and resulted in weak scattering curves. The molecular masses estimated from the 4- and 13-mg·mL^{-1} samples were identical. For consistency with the $XfDsbC_{Red}$ samples, we selected the $XfDsbC_{N\text{-}Red}$ curves collected at 4 mg·mL^{-1} for further analyses. As observed for $XfDsbC_{Red}$, the $XfDsbC_{N\text{-}Red}$ protein samples suffered radiation damage. Therefore, only the first curve was selected (Fig. 4C). The $XfDsbC_{N\text{-}Red}$ Guinier region is displayed in Fig. 4C (inset). From the Guinier analysis, an Rg of 35.4 Å was calculated. The Kratky plot was also evaluated (Fig. 4B) and showed a defined maximum with smaller q values than those of the $XfDsbC_{Red}$ maximum, which indicates a larger $XfDsbC_{N\text{-}Red}$ scattering particle. The $XfDsbC_{N\text{-}Red}$ molecular mass obtained in the absence of TCEP was estimated to be 117 kDa, suggesting that, in the absence of reducing agent, an XfDsbC tetramer is formed in solution. The $XfDsbC_{N\text{-}Red}$ $P(r)$ had a D_{max} of 130 Å (Fig. 4D), and the distance peak was concentrated at small distances, indicating a prolate $XfDsbC_{N\text{-}Red}$ structure. A second estimation of the Rg calculated from the $P(r)$ was 38.4 Å, which is consistent with the values obtained in the Guinier analysis.

Table 1. Hydrodynamic diameters (D_h), percentage of sample polydispersity (% Pd), estimated molecular weights from the measured radius (MW-R), percentage of sample intensity (% Int) and estimated relative amount of mass (% Mass) of each species determined from DLS analysis of XfDsbC in the presence ($XfDsbC_{N\text{-}Red}$) or absence ($XfDsbC_{Red}$) of a reducing agent.

Sample	D_h (nm)	% Pd	MW-R (kDa)	% Int	% Mass
$XfDsbC_{N\text{-}Red}$	4.6	9.5	119	73	99.6
$XfDsbC_{Red}$[a]	3.8	5.8	75	72	99.5

[a] To ensure complete protein reduction, XfDsbC was incubated with a freshly prepared solution of TCEP at a final concentration of 3 mM for 1 h before the DLS experiments.

The XfDsbC tetramer appears to be compact and distinct from the joining of two dimers

The monomeric XfDsbC homology model constructed with the I-TASSER server exhibited similarities to the EcDsbC [18] and *Haemophilus influenzae* DsbC (HiDsbC) [27] proteins. The amino acid sequence

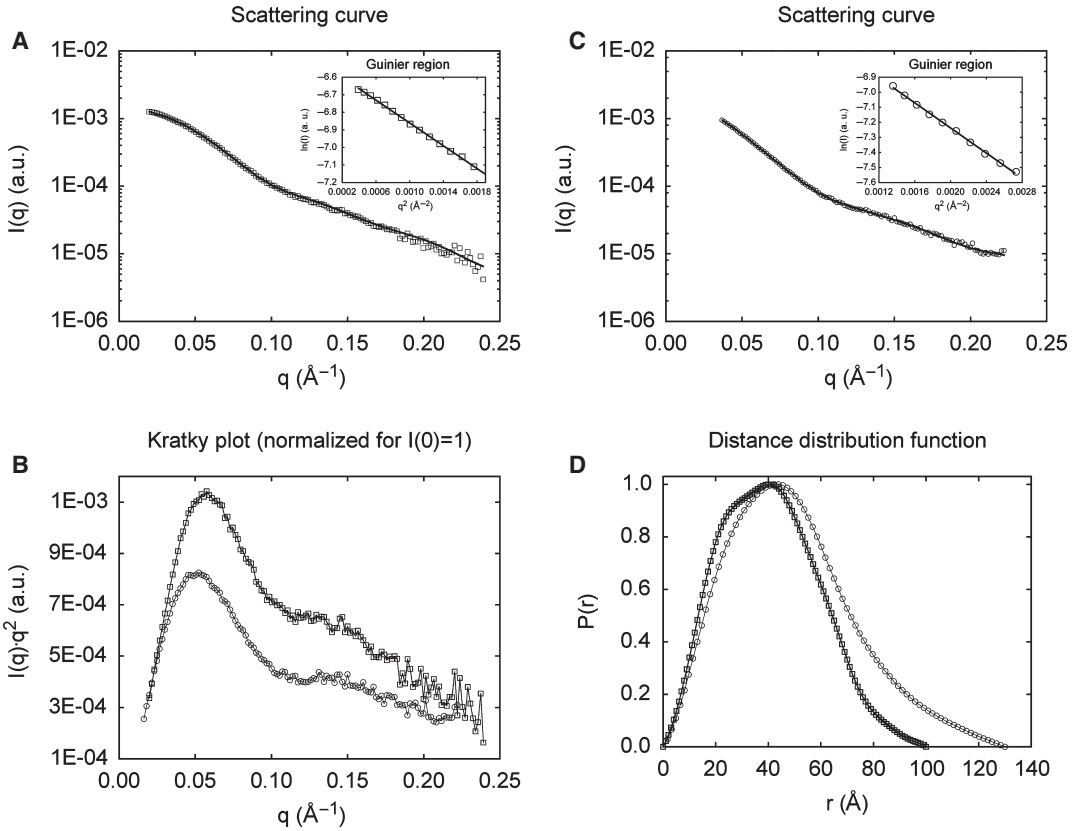

Fig. 4. XfDsbC SAXS analysis under reducing and nonreducing conditions. XfDsbC SAXS data analysis from samples collected in the presence ($XfDsbC_{Red}$) or absence ($XfDsbC_{N\text{-}Red}$) of TCEP. (A) $XfDsbC_{Red}$ scattering curve (open squares) and BUNCH curve (solid line) fitting. (B) Kratky plots. (C) $XfDsbC_{N\text{-}Red}$ scattering curve (open circles) and SASREF curve (solid line) fitting. The Guinier regions are shown in the insets A and C. (D) distance distribution functions [*P*(r)]. The Kratky plots and [P(r)] were calculated for *q* values in the range 0.0197–0.3008 Å^{-1} for $XfDsbC_{Red}$ and 0.0351–0.2152 Å^{-1} for $XfDsbC_{N\text{-}Red}$. The $XfDsbC_{Red}$ and $XfDsbC_{N\text{-}Red}$ plots are shown as squares and circles, respectively.

similarity of these two proteins to XfDsbC is approximately 35%. As observed in the structures of EcDsbC and HiDsbC, the constructed XfDsbC model displays two distinguishable domains: the dimerization and catalytic domains. The dimerization domain is small and is composed of 58 residues (residues 20–77) that form a β-strand, a turn and an α-helix. The catalytic domain is the largest domain and displays a thioredoxin-like fold. The XfDsbC catalytic domain is comprised of residues 86–244 and harbours the active site cysteine residues (Cys143 and Cys146 in XfDsbC, which correspond to Cys98 and Cys101 in EcDsbC). The catalytic domain is connected to the dimerization domain by a poorly modelled hinge. To construct the XfDsbC dimer, the 3D structure of the constructed monomer homology model was superimposed on the crystal structure of the EcDsbC dimer (PDB code: 1EEJ). A second XfDsbC chain was generated and superimposed on the remaining EcDsbC monomer. The putative XfDsbC dimer interface was proposed based on the high-resolution structures, chimeric constructs and site-directed mutagenesis of other DsbC dimeric proteins [18,26–28]. The dimerization domains of EcDsbC and HiDsbC are primarily connected by hydrogen-bond interactions formed by main chain residues from two external anti-parallel β-strands. An ionic interaction between EcDsbC His45 and Asp53 also contributes to the stability of the dimer and protein isomerase activity [26,29]. Therefore, the conservation of this characteristic interface in the XfDsbC structure was investigated. According to the XfDsbC homology model, XfDsbC has an external β-strand in its dimerization domain. The β-strand enables anti-parallel main chain contacts between the two XfDsbC dimerization domains and likely involves residues 68–77. An arginine (Arg68) and an aspartate (Asp77) residue are located on the extremities of this β-strand. Because Arg and Asp are oppositely charged, it is possible that ionic interactions help to stabilize the XfDsbC dimer, as observed in EcDsbC [26,29].

Based on this potential XfDsbC dimeric interface, the XfDsbC dimer was modelled according to the experimental XfDsbC low-resolution scattering curve. In this step, the XfDsbC dimerization domains and catalytic domains were provided as individual chains to the software suite BUNCH. Restraints were imposed to prevent the domains from being too far apart and to maintain the dimerization interface. A maximum distance from the centre of mass of each dimerization domain and catalytic domain to residues 68–77 of the two dimerization domains was set to maintain the dimerization interface and preserve the proximity of the catalytic domains and dimerization domains. The linker region (residues 78–85) that connects the dimerization and catalytic domains was removed from the input sequence, and the software was allowed to model these flexible regions. More than 40 XfDsbC atomic models were generated by BUNCH, and these models showed a good fit to the experimental SAXS curves, with chi-squared values of approximately 2.5. These models were visually inspected and sorted into three major groups that primarily differed in the orientation of the catalytic domains. In one of these groups, the catalytic Cys125 was turned away from the catalytic cleft and was exposed to the solvent, which would likely limit the activity of the protein. The cleft formed by the two catalytic domains has been suggested to play an important role in substrate recognition and protein activity [26] because the catalytic cysteine residue is oriented in the direction of this cleft in the known DsbC crystal structures. Therefore, the models with the cysteine facing away from the cleft were considered to have an improbable catalytic domain orientation and were discarded. The remaining models were carefully inspected and further clustered into two groups. The first group was comprised of models that followed the dimerization and catalytic domain orientations predicted by known DsbC crystal structures (Fig. 5A). The second group included models with intertwined dimerization and catalytic domains (named 'inverted dimers'; Fig. S2). It was difficult to evaluate the correctness of these two groups of XfDsbC dimer models because both models are possible given the low-resolution data. However, because the models in the first group were most similar to the reported DsbC crystal structures, one of the dimers from this group of models was selected for further analysis (Fig. 5A).

The selected XfDsbC SAXS dimer model is similar to the EcDsbC dimer crystal structure (PDB code: 1EEJ). The dimerization domains are connected by contacts mediated by two β-strand-like secondary structural elements on the surface of each dimerization domain. The dimer displays a V-shaped conformation,

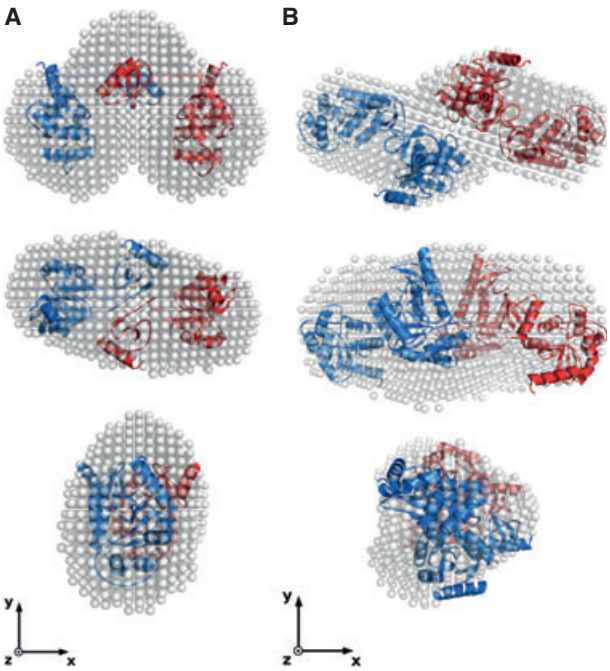

Fig. 5. The oligomeric assembly of XfDsbC responds to the environmental redox state *in vitro*. The suggested XfDsbC dimer (A) and tetramer (B) were modelled based on SAXS curves. The 3d XfDsbC atomic model for the dimer was generated using BUNCH, whereas the tetramer was modelled with SASREF. P2 symmetry was imposed in both cases. In both strategies, the dimerization and catalytic domains were inputted as independent entities, and only a few constraints were imposed for model generation. The low-resolution protein envelopes, which were constructed with DAMMIF software, are shown as semi-transparent whitish spheres superimposed on the atomic models. The middle views are rotated by 90° around the *x*-axis, clockwise in (A) and counterclockwise in (B). The bottom views in both panels are rotated 90° clockwise around the *y*-axis. The figures were generated USING PYMOL (Schrodinger LLC).

and a potential catalytic cleft is formed between the two catalytic domains. This cleft has an internal angle of approximately 60°, suggesting that XfDsbC is slightly closed in comparison to EcDsbC (internal cleft angle of approximately 70°). The catalytic XfDsbC cysteine residue (Cys143) and its disulfide bond partner (Cys146) are positioned close to the catalytic cleft. However, the adjacent structural cysteines (Cys186 and Cys208) are oriented in opposite directions and are slightly exposed to the solvent.

It was not possible to model the XfDsbC tetramer using a rigid-body fit for the SAXS-modelled XfDsbC dimer described above, which suggests that the XfDsbC dimer undergoes domain orientation and/or conformational changes to form the tetramer. Therefore, in an attempt to model a putative XfDsbC tetramer, four

XfDsbC dimerization and catalytic domains were inputted into SASREF software as individual chains. Using this strategy, SASREF was able to model an XfDsbC tetramer using only a few constraints.

The models obtained from different runs were judged to be similar by visual inspection. One of the XfDsbC tetrameric models is presented in Fig. 5B. The chi-squared value obtained for the comparison of the $XfDsbC_{N\text{-}Red}$ SAXS curve with the modelled tetramer is 1.6, which indicates an excellent fit and the correctness of the model. The modelled XfDsbC tetramer is formed by interchain contacts between two catalytic domains from different dimers and likely involves domain reorientation, as noted above.

Curiously, the XfDsbC tetrameric models were similar to the DsbC oligomeric structures generated by applying symmetric operations to DsbC crystal structures (Fig. S3). This observation may support the possibility that larger oligomers of DsbC proteins can form.

Discussion

The XfDsbC protein was annotated in the *X. fastidiosa* 9a5c genome as being involved in pathogenicity, adaptation and survival [30]. Functional and structural studies of proteins in this category have helped determine how this bacterium has adapted to plant hosts and provide a better understanding of the mechanisms underlying pathogenicity and bacterial virulence [31–34].

Biofilm formation is considered to be the primary mechanism of pathogenicity by *X. fastidiosa* [35]. The phases of *X. fastidiosa* biofilm development have been defined previously [34,36]. The initial adhesion phase of the cells to the substrate occurs after 3–5 days. Within 10 days, micro-colonies are formed, followed by a maturation phase that occurs between 15 and 20 days after adhesion. The development of the biofilm architecture begins at approximately 15 days, and the biofilm is fully mature within 20 days. The last stage of biofilm formation, the dispersion phase, occurs between 25 and 30 days after adhesion.

We confirmed that XfDsbC is involved in bacterial pathogenicity by demonstrating its expression during *X. fastidiosa* biofilm formation. Interestingly, XfDsbC is poorly expressed during *X. fastidiosa* planktonic growth, suggesting that, under these conditions, the disulfide bond isomerization pathway is largely not required for bacterial survival. The frequency of the formation of non-native disulfide bonds by DsbA is low under normal bacterial growth conditions [37], which explains the minimal requirement for XfDsbC during *X. fastidiosa* planktonic growth. Biofilm growth provides greater adaptive advantages than planktonic growth by coordinating the growth rate, which provides the cells with increased resistance to antimicrobial agents, such as metals [38]. Thus, stress response pathways, including mechanisms that promote survival, have a major role in the success of bacterial biofilm formation [39]. The disulfide bond isomerization pathway in which XfDsbC plays its primary role comprises one such survival mechanism because it is directly involved in protein folding [2–5,10].

Cells exhibit different gene expression and metabolic profiles during biofilm and planktonic growth [34,40]. In the present study, we demonstrated, by direct immunodetection, that XfDsbC is differentially expressed during *X. fastidiosa* planktonic and biofilm growth. Interestingly, in response to metal stress, planktonic *X. fastidiosa* overexpresses XfDsbC, with expression levels similar to those observed in mature biofilms. Our findings reveal that *X. fastidiosa* can use XfDsbC *in vivo* as a response to oxidative stress, which is corroborated by the finding that XfDsbC is able to complement a *dsbC*-null *E. coli* mutant under similar stress conditions. However, during the mature biofilm stage, copper does not appear to affect the expression profile of XfDsbC. At this stage, the complete structure of the biofilm makes the cells less responsive to changes in the external environment [38–40]. Therefore, the expression of XfDsbC at the mature biofilm stage in the presence or absence of copper reflects the response to bacterial growth under biofilm growth conditions, as opposed to a specific response to metal stress. The initial stage of *X. fastidiosa* biofilm development is marked by the production of many cysteine-rich proteins, including pili and adhesin proteins [34]. The increased expression of XfDsbC during biofilm formation may be related to the increased expression of cysteine-rich proteins and the need to fold these proteins correctly. Moreover, the differences observed between biofilms in the presence and absence of copper appear to indicate that the bacterial cells are more susceptible to changes in the external environment during microcolony formation and biofilm dispersal; increased XfDsbC expression appears to be a coordinated cellular action in these phases. At the stage of cell adhesion to the substrate, the cells may rely on mechanisms outside of the isomerization pathway to respond to oxidative stress, resulting in a decreased level of XfDsbC expression under these conditions.

In addition to disulfide bond reductase and isomerase activity, DsbC proteins have chaperone activity [12,13]; however, the mechanism of this activity is not completely understood for DsbC. One intrinsic feature

of a chaperone-like protein is the formation of large oligomers that facilitate interactions between proteins and their substrates [41]. The detection of XfDsbC tetramers by DLS and SAXS under nonreducing conditions may be evidence of chaperone activity. However, whether this oligomeric state occurs *in vivo* is unclear.

DsbC homologues have always been described as homodimers [18,26–28], and their disulfide bond reduction/isomerization activity is partly correlated with this state [2–5]. However, Arredondo *et al.* [26] observed evidence for a linked EcDsbC with a single active thioredoxin domain in a tetrameric state using multi-angle light scattering. The hydrodynamic radius of the tetramer was 4.4 nm, which is not consistent with the radius of the dimer (3.8 nm) and suggests that the tetramer is a compact molecule [26]. These results are in accordance with our findings of DLS and, similarly, the compact form of EcDsbC tetramer appears to be consistent with the XfDsbC tetramer that we observed *in vitro* in the SAXS analysis.

We did not observe any differences between the reduced and nonreduced forms of XfDsbC by size-exclusion chromatography or native gel electrophoresis. However, DLS and SAXS analyses demonstrated the influence of a reducing agent in the folding state of XfDsbC. Thus, it is possible that the reducing agent-mediated XfDsbC dimer-tetramer modulation is not directly linked to disulfide bond formation at the tetramer interface. Rather, it appears that, under nonreducing conditions, certain amino acid residues may be exposed, promoting XfDsbC tetramer formation. By contrast, under reducing conditions, disulfide bond breakage hinders or hides this interface. The current low-resolution data do not clarify the mechanism that guides XfDsbC tetramer assembly.

Based on fluorimetry analysis in which the disulfide reduction increases fluorescence emission, we can assert that changes in the folding state of XfDsbC are related to disulfide bond formation between Cys186 and Cys208, which are equivalent to Cys141 and Cys163 in EcDsbC [18]. Interestingly, the disulfide bond formed between these cysteine residues has a substantial structural role in EcDsbC folding [24]. Therefore, the absence of differences in XfDsbC behaviour by size-exclusion chromatography and native gel electrophoresis could be explained by the weakness of the tetramerization interface, which may not be maintained under the drag and pressure conditions of chromatography and electrophoresis because a tetrameric form of XfDsbC was observed *in vitro* by chemical cross-linking at low protein concentration only under the nonreduced condition.

Previous studies in which amino acid residues important for EcDsbC dimerization were replaced have shown that the dimeric disulfide isomerase is converted into a monomeric protein that retains oxidase activity, similar to DsbA [29,42], suggesting that dimerization acts to protect the DsbC active sites from DsbB-mediated oxidation [29,43]. Tetramer formation may play a similar role for XfDsbC, for example, in preventing the reduction of the disulfide bonds. Bioinformatics estimates have revealed that more than 300 *E. coli* proteins that contain multiple cysteines are exported to the periplasm [44,45] and may be substrates for disulfide bond-forming enzymes [5]. Thus, the XfDsbC redox-dependent modulation observed *in vitro* may be involved in substrate recognition and specificity, comprising a role that has not been previously described for DsbC homologues.

Experimental procedures

Bacterial strain and *in vitro* growth conditions

X. fastidiosa subsp. *pauca* 9a5c [46] and *E. coli* strains DH5-α, C43 (DE3) (Avidis, Saint-Beauzire, France), JW2861 and BW25113 [47] were used in the present study. Before *in vitro* culture, the *X. fastidiosa* cells were inoculated into susceptible sweet orange trees to maintain their pathogenicity [34]. The infected plants developed symptoms typical citrus of variegated chlorosis, and the bacteria were isolated. *X. fastidiosa* was grown in Periwinkle Wilt media [48] at 130 r.p.m. and 28 °C, and the *E. coli* strains were cultured in LB or Brain-Heart Infusion Broth (BHI; HiMedia, Mumbai, India) media at 200–300 r.p.m. and 25–37 °C, with antibiotic supplementation as necessary. The *X. fastidiosa* biofilm and planktonic cells were obtained using a protocol established by De Souza *et al.* [36] and a sublethal copper shock with 1 mM $CuSO_4$ was applied for 24 h as indicated.

Cloning, expression and purification

The coding sequence of the *xfdsbC* ORF *Xf*1177 (798 bp) was amplified from *X. fastidiosa* genomic DNA by PCR with the specific oligonucleotides Xf1177petF (5′-CC AAACATATGTACCGCCTTATCGTCGCCTTG-3′) and Xf1177petR (5′-AAACTCGAGGCCCCCTTTAGCTGTT GCGG-3′), which contained *Nde*I and *Xho*I restriction sites, respectively. The PCR amplification product was cloned into the pET29a(+) (Novagen, Madison, WI, USA) expression vector, which added a C-terminal six-histidine tag to the coding sequence. Sequence analysis of the cloned vector did not reveal any base substitutions. To overexpress XfDsbC in *E. coli* C43 (DE3) cells, the cells were grown at 37 °C in 1 L of LB containing 30 $\mu g \cdot mL^{-1}$ kanamycin until

D_{600} of 0.6–0.8 was reached. The expression of the recombinant protein was induced by the addition of 5.6 mM lactose followed by cultivation for 18 h at 25 °C and 200 r.p.m. The culture was harvested by centrifugation (3000 ***g*** for 15 min at 4 °C) and then the cell pellets were resuspended in 50 mL of buffer A (50 mM Tris-HCl, pH 7.5, 300 mM NaCl) plus 1 mg·mL^{-1} lysozyme and 1 mM phenylmethanesulfonyl fluoride (Sigma, St Louis, MO, USA) and incubated on ice for 30 min. The cells were disrupted by sonication, and the unbroken cells and debris were removed by centrifugation (27 000 ***g*** for 40 min at 4 °C). The XfDsbC protein was purified in a single chromatographic step on a Ni-NTA column (Qiagen, Hilden, Germany) equilibrated in buffer A. The purified XfDsbC protein was eluted with five column volumes of buffer A containing 250 mM imidazole, and the purity was estimated using SDS/PAGE. The affinity-purified XfDsbC sample was dialyzed overnight against buffer B (50 mM Tris-HCl, pH 7.5, 150 mM NaCl) at 4 °C. The determination of the redox states of purified XfDsbC was achieved using Ellman's method [49]. The protein concentration was spectrophotometrically determined and calculated from the A_{280} with a molar absorption coefficient (ε_{280}) of 23 630 M^{-1}·cm^{-1}, assuming that all Cys residues were oxidized, or 23 380 M^{-1}·cm^{-1}, assuming that all Cys residues were reduced.

Biochemical assays and disulfide bond isomerization *in vivo*

The *in vitro* thiol-disulfide reductase activity of XfDsbC was determined by measuring the turbidity increase at 650 nm resulting from insulin reduction in accordance with published procedures [50]. EcDsbC purified from the JW2861 clone, as obtained from the ASKA library [51], was used as a positive control in these tests. Reductase activity was expressed as the ratio of the slope of the linear portion of the turbidity curve to the lag time [52]. In addition, the XfDsbC disulfide bond isomerase activity was assessed *in vivo* using a functional complementation assay based on copper sensitivity [21]. The *xfdsbC* gene was cloned into the pBAD24 vector [53] using the oligonucleotides Xf1177badF (5′-ATCCATGGGTTACCGCCTTATC GTCG-3′) and Xf1177badR (5′-AATGTCGACTCAGCC CCCTTTAGCT-3′), which contained *Nco*I and *Sal*I restriction sites, respectively. pBAD24-*xfdsbC* or pBAD24 empty vector was transformed into the *E. coli* JW2861 strain, which is a *dsbC* deletion mutant derived from the wild-type BW25113 strain. Both strains were kindly provided by the National BioResource Project (NIG, Mishima, Japan). For the copper sensitivity assay, the strains (wild-type, *dsbC*$^-$ and *dsbC*$^-$ containing pBAD24-*xfdsbC* or the empty vector) were grown overnight in LB containing 30 μg·mL^{-1} chloramphenicol, 100 μg·mL^{-1} ampicillin or 30 μg·mL^{-1} kanamycin (depending on the strain) at 37 °C and 300 r.p.m. The cultures were then diluted 1 : 100 in BHI media supplemented with the appropriate antibiotic and grown at 37 °C and 300 r.p.m. until D_{600} of 0.8 was reached. The *dsbC* phenotype was tested by spotting 5 μL of 10-fold serial dilutions onto BHI agar plates with the appropriate antibiotic containing 0, 4 and 8 mM $CuCl_2$ with and without 0.002% w/v L-arabinose. The plates were incubated overnight at 37 °C, and the ability of XfDsbC to restore the wild-type phenotype was analyzed. We reintroduced wild-type EcDsbC, which was expressed from the pCA24N plasmid [51], into the *dsbC*$^-$ strain as a positive control for functional complementation. All of the spot titrations were performed in triplicate, and XfDsbC expression in the *dsbC*$^-$ strain was confirmed by western blot analysis.

Extraction of total protein from *X. fastidiosa* biofilm and planktonic cells

X. fastidiosa biofilm and planktonic cells were collected after 3, 5, 10, 15, 20 and 30 days of growth. To assess the differential metal stress responses of the biofilm and planktonic cells, both cell types were exposed to a sublethal copper shock for 24 h with 1 mM $CuSO_4$. Biofilm and planktonic cells exposed or not exposed to $CuSO_4$ were sampled at various time points, and total protein was extracted from each sample. For total protein extraction, the biofilm and planktonic cells from each treatment were collected and resuspended in 1 mL of extraction buffer (50 mM Tris-HCl, pH 8.0, 25 mM NaCl, 5 mM EDTA and 2% Triton X-100) containing 1 mg·mL^{-1} lysozyme and 1 mM phenylmethanesulfonyl fluoride. The samples were placed on ice for 20 min and lysed by sonication, followed by centrifugation (10 000 ***g*** for 10 min at 4 °C). The total protein concentration of each protein sample was normalized with a micro BCA protein assay kit (Thermo Fisher Scientific Inc., Waltham, MA, USA) before SDS/PAGE analysis. A BSA standard curve was utilized for the total protein concentration comparison. The standard curve exhibited an R^2 of 0.989.

XfDsbC immunodetection during *X. fastidiosa* biofilm and planktonic growth

Polyclonal antibodies against XfDsbC were produced by Rheabiotech (Campinas, Brazil) and used in the XfDsbC immunodetection assays. For western blot analysis, approximately 105 μg of total *X. fastidiosa* protein from different biofilm developmental phases and planktonic growth cultures were separated using 12% SDS/PAGE. After electrophoresis, the proteins were transferred to nitrocellulose membranes (Immobilon^{TM}-Nc; Sigma) using a Trans-Blot Semi-Dry Transfer Cell (Bio-Rad, Hercules, CA, USA) in accordance with the manufacturer's instructions. XfDsbC was detected with a 1 : 4000 dilution of anti-XfDsbC and a 1 : 8000 dilution of alkaline phosphatase-conjugated

anti-rabbit IgG (Santa Cruz Biotechnology Inc., Santa Cruz, CA, USA). The membranes were developed with NBT/BCIP chromogenic substrates (Promega, Madison, WI, USA). Three independent experiments were performed for each biological treatment to assess potential variations in protein transfer. The signal intensity was quantified using EDAS 290 software (Kodak, Rochester, NY, USA), and the resulting values were subjected to statistical analysis ($P \leq 0.05$, *t*-test).

Native gel electrophoresis analysis

Nondenaturing PAGE was performed under the conditions previously described for a pH range of 8.6–10.6 [54]. XfDsbC (p*I* = 9.01) protein samples (approximately 60 μg) in the presence and absence of 3 mM TCEP reducing agent were analyzed using 7.5% native gel electrophoresis with aldolase (p*I* = 6.1, 158 kDa) and conalbumin (p*I* = 5.9, 75 kDa) (GE Healthcare, Uppsala, Sweden) as standards.

CD

The CD spectra of the recombinant XfDsbC were collected on a Jasco J-810 Spectropolarimeter dichrograph (Japan Spectroscopic, Tokyo, Japan). The far-UV CD spectra were generated with XfDsbC at an approximate concentration of 5 μM in 10 mM sodium phosphate buffer at pH 7.5 with 0 or 3 mM TCEP. The assays were performed in a quartz cuvette with a path length of 1 mm, and 10 accumulations within the range 260–190 nm at a rate of 50 nm·min^{-1} at 24 °C were recorded for each sample and the mean was determined. The deconvolution and statistical analysis of the CD spectra were performed using DICHROWEB [55].

Size-exclusion chromatography

Gel filtration chromatography was performed using a prepacked Superdex 200 HR10/30 (GE Healthcare) column. After equilibration of the column with buffer B, samples (approximately 750 μg) containing 0 or 3 mM TCEP were loaded at a flow rate of 0.5 mL·min^{-1}. The Superdex column was calibrated using HMW and LMW calibration kits (GE Healthcare) as standard molecular weight markers.

DLS

DLS measurements were performed on a DynaPro instrument (Protein Solutions Inc., Charlottesville, VA, USA). XfDsbC samples at a concentration of 1 and 4 mg·mL^{-1} in the absence or presence of 3 mM TCEP were analyzed in buffer B. $XfDsbC_{N\text{-}Red}$ or $XfDsbC_{Red}$ samples (approximately 100 μL) were placed in a quartz cell and DLS measurements were taken at 4 °C. At least 100 acquisitions of 5 s were collected for each condition tested.

Glutaraldehyde cross-linking

The oligomeric state of purified XfDsbC was determined *in vitro* by chemical cross-linking with glutaraldehyde. The protein samples (approximately 5 μM protein in 20 mM Hepes buffer, pH 7.5, in a total volume of 100 μL) in the presence or absence of 3 mM TCEP were incubated on ice for 5 min with increasing concentrations (0–0.1%) of a freshly prepared solution of glutaraldehyde. The reactions were stopped by adding 10 μL of 1 M Tris-HCl, pH 8.0, and the products were evaluated by SDS/PAGE and western blot analysis using polyclonal antibodies against XfDsbC.

Tryptophan fluorescence measurements

The tryptophan fluorescence spectra of XfDsbC were measured on an ISS K2 Fluorescence Spectrometer (ISS, Champaign, IL, USA). Three independent experiments were performed using 5 μM XfDsbC in the presence and absence of 3 mM TCEP in buffer B. Excitation was performed at a fixed wavelength of 280 nm, and emission spectra were recorded in the range 300–400 nm. The fluorescence contribution from the blank solutions containing the reducing agent or not were subtracted from that of the samples reduced or nonreduced, respectively.

SAXS data collection, processing and model construction

XfDsbC samples were submitted for SAXS data collection. XfDsbC at concentrations of 1, 4, 7 and 13 mg·mL^{-1} in buffer B was incubated with 0 or 3 mM TCEP for 3 h before the SAXS experiments. The samples were centrifuged at 13 000 ***g*** at 4 °C before use in the SAXS experiments. The SAXS data collection was performed at the SAXS-1 beamline at the Brazilian National Synchrotron Light Laboratory (LNLS, Campinas, Brazil) [56] with a Pilatus (300 K; 84 × 107 mm) 2D detector (Dectris Ltd, Baden, Switzerland) and a monochromatic X-ray beam with a wavelength of 1.3808 Å. The sample-to-detector distance was adjusted to 1101.50 mm to cover a momentum transfer interval of $0.0158 < q < 0.4426$ Å^{-1}, where $q = [(4\pi)/(\lambda)]\sin\theta$ and 2θ is the scattering angle. Individual XfDsbC samples were carefully loaded into cells made of two thin, parallel mica windows and maintained at 4 °C during the measurements. The protein samples and buffer solution were exposed to the X-ray beam in 1- to 5-min frames. At least 10 successive frames were recorded for each protein concentration and TCEP condition.

The data reduction was performed using FIT2D [57] with radial integration of the collected images, and normalization was performed relative to the intensity of the transmitted beam after buffer scattering subtraction. The SAXS data analyses were performed using ATSAS software [58].

The Rg and scattering intensity at zero angle [$I(0)$] were calculated using the indirect Fourier transform method implemented in GNOM software [58], which also calculates the distance distribution function $P(r)$ and allows the assessment of D_{max} and molecule anisometry. Kratky plots [$q^2I(q) \times q$] [59] were also generated to evaluate the conformational variability of the protein in solution. The molecular weight of the protein was estimated using the SAXS MoW algorithm [25].

Ab initio dummy bead models were calculated from the experimental curves using DAMMIN and DAMMIF [56,60]. Different point-group symmetries (P1, P2 and P4) were imposed, and the best results were obtained with P2 symmetry. The final low-resolution 3D envelope, which represents the protein, was generated by averaging independent runs with DAMAVER and DAMFILT software [61] in automatic mode. The individual and mean SAXS envelopes were visually inspected.

In parallel with the *ab initio* methods used to construct the low-resolution envelope from the experimental curve, rigid-body modelling was performed. First, a monomeric XfDsbC 3D homology model was obtained using the I-TASSER server [62]. To assemble possible XfDsbC dimers and tetramers, the I-TASSER XfDsbC models were superimposed on the EcDsbC crystal structure (PDB code: 1EEJ) using PYMOL (Schrodinger LLC, New York, NY, USA). Possible XfDsbC dimerization interfaces were suggested based on the EcDsbC dimeric structure [18]. The theoretical dimeric XfDsbC atomic model was first modelled onto the SAXS curve using BUNCH [63]. In this procedure, an XfDsbC monomer was presented to the software with separate dimerization and catalytic domains, and few restraints were imposed in the reconstruction of the XfDsbC dimer.

The XfDsbC tetramer models were constructed using SASREF software [64]. For this task, the catalytic and dimerization domains were separately provided to the software, and restrictions on the shortest and longest distances for the independent domains were imposed. The dimerization interface was restricted based on the results obtained with the XfDsbC dimer model.

The discrepancy (χ) between the experimental data and the theoretical scattering curves computed for each possible atomic model was assessed using CRYSOL software [64]. Conventionally, the χ parameter, which is provided by CRYSOL, is used as a measurement of the goodness of fit to the experimental data. The structural alignments were performed using SUPCOMB software [65].

Acknowledgements

The work described in the present study was supported by grants from the Fundação de Amparo à Pesquisa do Estado de São Paulo (FAPESP, Process 01/07533-7). C.A.S. was the recipient of a graduate fellowship from FAPESP (Process 08/55690-3); A.P.S. and R.A. are recipients of a research fellowship from the Conselho Nacional de Desenvolvimento Científico e Tecnológico (CNPq). We gratefully acknowledge the Laboratório Nacional de Luz Síncrotron (LNLS, Campinas, Brazil) for providing beamline time. We would also like to thank Mateus B. Cardoso for help with the SAXS experiments and the Laboratório de Espectroscopia e Calorimetria (LEC) and Laboratório Nacional de Biociências (LNBio, Campinas, Brazil) for support with the spectroscopic studies. The authors declare that there are no conflicts of interest.

References

1 Thakur KG, Praveena T & Gopal B (2010) Structural and biochemical bases for the redox sensitivity of *Mycobacterium tuberculosis* RslA. *J Mol Biol* **397**, 1199–1208.
2 Sato Y & Inaba K (2012) Disulfide bond formation network in the three biological kingdoms, bacteria, fungi and mammals. *FEBS J* **279**, 2262–2271.
3 Messens J & Collet JF (2006) Pathways of disulfide bond formation in *Escherichia coli*. *Int J Biochem Cell Biol* **38**, 1050–1062.
4 Gleiter S & Bardwell JC (2008) Disulfide bond isomerization in prokaryotes. *Biochim Biophys Acta* **1783**, 530–534.
5 Kadokura H & Beckwith J (2010) Mechanisms of oxidative protein folding in the bacterial cell envelope. *Antioxid Redox Signal* **13**, 1231–1246.
6 Pedone E, Limauro D, D'Ambrosio K, De Simone G & Bartolucci S (2010) Multiple catalytically active thioredoxin folds: a winning strategy for many functions. *Cell Mol Life Sci* **67**, 3797–3814.
7 Wunderlich M & Glockshuber R (1993) Redox properties of protein disulfide isomerase (DsbA) from *Escherichia coli*. *Protein Sci* **2**, 717–726.
8 Warwicker J (1998) Modeling charge interactions and redox properties in DsbA. *J Biol Chem* **273**, 2501–2504.
9 Hennecke J, Sebbel P & Glockshuber R (1999) Random circular permutation of DsbA reveals segments that are essential for protein folding and stability. *J Mol Biol* **286**, 1197–1215.
10 Rietsch A, Belin D, Martin N & Beckwith J (1996) An *in vivo* pathway for disulfide bond isomerization in *Escherichia coli*. *Proc Natl Acad Sci USA* **93**, 13048–13053.
11 Hiniker A & Bardwell JC (2004) *In vivo* substrate specificity of periplasmic disulfide oxidoreductases. *J Biol Chem* **279**, 12967–12973.
12 Chen J, Song JL, Zhang S, Wang Y, Cui DF & Wang CC (1999) Chaperone activity of DsbC. *J Biol Chem* **274**, 19601–19605.

13 Liu X & Wang CC (2001) Disulfide-dependent folding and export of *Escherichia coli* DsbC. *J Biol Chem* **276**, 1146–1151.
14 Heras B, Shouldice SR, Totsika M, Scanlon MJ, Schembri MA & Martin JL (2009) DSB proteins and bacterial pathogenicity. *Nat Rev Microbiol* **7**, 215–225.
15 Rietsch A, Bessette P, Georgiou G & Beckwith J (1997) Reduction of the periplasmic disulfide bond isomerase, DsbC, occurs by passage of electrons from cytoplasmic thioredoxin. *J Bacteriol* **179**, 6602–6608.
16 Nakasako M, Maeno A, Kurimoto E, Harada T, Yamaguchi Y, Oka T, Takayama Y, Iwata A & Kato K (2010) Redox-dependent domain rearrangement of protein disulfide isomerase from a thermophilic fungus. *Biochemistry* **49**, 6953–6962.
17 Wilkinson B & Gilbert HF (2004) Protein disulfide isomerase. *Biochim Biophys Acta* **1699**, 35–44.
18 McCarthy AA, Haebel PW, Törrönen A, Rybin V, Baker EN & Metcalf P (2000) Crystal structure of the protein disulfide bond isomerase, DsbC, from *Escherichia coli*. *Nat Struct Biol* **7**, 196–199.
19 Berkmen M, Boyd D & Beckwith J (2005) The nonconsecutive disulfide bond of *Escherichia coli* phytase (AppA) renders it dependent on the protein-disulfide isomerase, DsbC. *J Biol Chem* **280**, 11387–11394.
20 Vertommen D, Depuydt M, Pan J, Leverrier P, Knoops L, Szikora JP, Messens J, Bardwell JC & Collet JF (2008) The disulphide isomerase DsbC cooperates with the oxidase DsbA in a DsbD-independent manner. *Mol Microbiol* **67**, 336–349.
21 Hiniker A, Collet JF & Bardwell JC (2005) Copper stress causes an *in vivo* requirement for the *Escherichia coli* disulfide isomerase DsbC. *J Biol Chem* **280**, 33785–33791.
22 Lee RF, Derrick KS, Beretta MJG, Chagas CM & Rosetti V (1991) Citrus variegated chlorosis: a new destructive disease of citrus in Brazil. *Citrus Ind* **72**, 12–15.
23 Chang CJ, Garnier M, Zreik L, Rossetti V & Bové JM (1993) Culture and serological detection of the xylem-limited bacterium causing citrus variegated chlorosis and its identification as a strain of *Xylella fastidiosa*. *Curr Microbiol* **27**, 137–142.
24 Zapun A, Missiakas D, Raina S & Creighton TE (1995) Structural and functional characterization of DsbC, a protein involved in disulfide bond formation in *Escherichia coli*. *Biochemistry* **34**, 5075–5089.
25 Fischer H, Neto MD, Napolitano HB, Polikarpov I & Craievich AF (2010) Determination of the molecular weight of proteins in solution from a single small-angle X-ray scattering measurement on a relative scale. *J Appl Crystallogr* **43**, 101–109.
26 Arredondo SA, Chen TF, Riggs AF, Gilbert HF & Georgiou G (2009) Role of dimerization in the catalytic properties of the *Escherichia coli* disulfide isomerase DsbC. *J Biol Chem* **284**, 23972–23979.
27 Zhang M, Monzingo AF, Segatori L, Georgiou G & Robertus JD (2004) Structure of DsbC from *Haemophilus influenzae*. *Acta Crystallogr D Biol Crystallogr* **60**, 1512–1518.
28 Banaszak K, Mechin I, Frost G & Rypniewski W (2004) Structure of the reduced disulfide-bond isomerase DsbC from *Escherichia coli*. *Acta Crystallogr D Biol Crystallogr* **60**, 1747–1752.
29 Bader MW, Hiniker A, Regeimbal J, Goldstone D, Haebel PW, Riemer J, Metcalf P & Bardwell JC (2001) Turning a disulfide isomerase into an oxidase: DsbC mutants that imitate DsbA. *EMBO J* **20**, 1555–1562.
30 Simpson AJ, Reinach FC, Arruda P, Abreu FA, Acencio M, Alvarenga R, Alves LM, Araya JE, Baia GS, Baptista CS *et al.* (2000) The genome sequence of the plant pathogen *Xylella fastidiosa*. *Nature* **406**, 151–159.
31 Saraiva AM, Reis MA, Tada SF, Rosselli-Murai LK, Schneider DRS, Pelloso AC, Toledo MAS, Giles C, Aparicio R & de Souza AP (2009) Functional and small-angle X-ray scattering studies of a new stationary phase survival protein E (SurE) from *Xylella fastidiosa* – evidence of allosteric behaviour. *FEBS J* **276**, 6751–6762.
32 Toledo MAS, Schneider DRS, Azzoni AR, Favaro MTP, Pelloso AC, Santos CA, Saraiva AM & Souza AP (2011) Characterization of an oxidative stress response regulator, homologous to *Escherichia coli* OxyR, from the phytopathogen *Xylella fastidiosa*. *Protein Expr Purif* **75**, 204–210.
33 Santos CA, Beloti LL, Toledo MAS, Crucello A, Favaro MTP, Mendes JS, Santiago AS, Azzoni AR & Souza AP (2012) A novel protein refolding protocol for the solubilization and purification of recombinant peptidoglycan-associated lipoprotein from *Xylella fastidiosa* overexpressed in *Escherichia coli*. *Protein Expr Purif* **82**, 284–289.
34 Caserta R, Takita MA, Targon ML, Rosselli-Murai LK, de Souza AP, Peroni L, Stach-Machado DR, Andrade A, Labate CA, Kitajima EW *et al.* (2010) Expression of *Xylella fastidiosa* fimbrial and afimbrial proteins during biofilm formation. *Appl Environ Microbiol* **76**, 4250–4259.
35 de Souza AA, Takita MA, Coletta-Filho HD, Caldana C, Goldman GH, Yanai GM, Muto NH, de Oliveira RC, Nunes LR & Machado MA (2003) Analysis of gene expression in two growth states of *Xylella fastidiosa* and its relationship with pathogenicity. *Mol Plant Microbe Interact* **16**, 867–875.
36 de Souza AA, Takita MA, Coletta-Filho HD, Caldana C, Yanai GM, Muto NH, de Oliveira RC, Nunes LR & Machado MA (2004) Gene expression profile of the

plant pathogen *Xylella fastidiosa* during biofilm formation *in vitro*. *FEMS Microbiol Lett* **237**, 341–353.
37 Shouldice SR, Heras B, Walden PM, Totsika M, Schembri MA & Martin JL (2011) Structure and function of DsbA, a key bacterial oxidative folding catalyst. *Antioxid Redox Signal* **14**, 1729–1760.
38 Rodrigues CM, Takita MA, Coletta-Filho HD, Olivato JC, Caserta R, Machado MA & de Souza AA (2008) Copper resistance of biofilm cells of the plant pathogen *Xylella fastidiosa*. *Appl Microbiol Biotechnol* **77**, 1145–1157.
39 Sauer K, Rickard AH & Davies DG (2007) Biofilms and biocomplexity. *Microbe* **2**, 347–353.
40 Booth SC, Workentine ML, Wen J, Shaykhutdinov R, Vogel HJ, Ceri H, Turner RJ & Weljie AM (2011) Differences in metabolism between the biofilm and planktonic response to metal stress. *J Proteome Res* **10**, 3190–3199.
41 Hartl FU, Bracher A & Hayer-Hartl M (2011) Molecular chaperones in protein folding and proteostasis. *Nature* **475**, 324–332.
42 Ke H, Zhang S, Li J, Howlett GJ & Wang CC (2006) Folding of *Escherichia coli* DsbC: characterization of a monomeric folding intermediate. *Biochemistry* **45**, 15100–15110.
43 Inaba K, Murakami S, Suzuki M, Nakagawa A, Yamashita E, Okada K & Ito K (2006) Crystal structure of the DsbB-DsbA complex reveals a mechanism of disulfide bond generation. *Cell* **127**, 789–801.
44 Hiniker A, Ren G, Heras B, Zheng Y, Laurinec S, Jobson RW, Stuckey JA, Martin JL & Bardwell JC (2007) Laboratory evolution of one disulfide isomerase to resemble another. *Proc Natl Acad Sci USA* **104**, 11670–11675.
45 Dutton RJ, Boyd D, Berkmen M & Beckwith J (2008) Bacterial species exhibit diversity in their mechanisms and capacity for protein disulfide bond formation. *Proc Natl Acad Sci USA* **105**, 11933–11938.
46 Schaad NW, Postnikova E, Lacy G, Fatmi M & Chang CJ (2004) *Xylella fastidiosa* subspecies: *X. fastidiosa* subsp. [correction] fastidiosa [correction] subsp. nov., *X. fastidiosa* subsp. multiplex subsp. nov. & *X. fastidiosa* subsp. pauca subsp. nov. *Syst Appl Microbiol* **27**, 290–300.
47 Baba T, Ara T, Hasegawa M, Takai Y, Okumura Y, Baba M, Datsenko KA, Tomita M, Wanner BL & Mori H (2006) Construction of *Escherichia coli* K-12 in-frame, single-gene knockout mutants: the Keio collection. *Mol Syst Biol* **2**, 2006.0008.
48 Davis MJ, French WJ & Schaad NW (1981) Axenic culture of the bacteria associated with phony disease of peach and plum leaf scald. *Curr Microbiol* **5**, 311–316.
49 Ellman GL (1959) Tissue sulfhydryl groups. *Arch Biochem Biophys* **82**, 70–77.
50 Holmgren A (1979) Thioredoxin catalyzes the reduction of insulin disulfides by dithiothreitol and dihydrolipoamide. *J Biol Chem* **254**, 9627–9632.
51 Kitagawa M, Ara T, Arifuzzaman M, Ioka-Nakamichi T, Inamoto E, Toyonaga H & Mori H (2005) Complete set of ORF clones of *Escherichia coli* ASKA library (a complete set of *E. coli* K-12 ORF archive): unique resources for biological research. *DNA Res* **12**, 291–299.
52 Martínez-Galisteo E, Padilla CA, García-Alfonso C, López-Barea J & Bárcena JA (1993) Purification and properties of bovine thioredoxin system. *Biochimie* **75**, 803–809.
53 Guzman LM, Belin D, Carson MJ & Beckwith J (1995) Tight regulation, modulation & high-level expression by vectors containing the arabinose PBAD promoter. *J Bacteriol* **177**, 4121–4130.
54 Gallagher SR (2001) One-dimensional electrophoresis using nondenaturing conditions. *Curr Protoc Protein Sci* **10**, 10.3.1–10.3.11.
55 Whitmore L & Wallace BA (2004) DICHROWEB, an online server for protein secondary structure analyses from circular dichroism spectroscopic data. *Nucleic Acids Res* **32**, W668–W673.
56 Kellermann G, Vicentin F, Tamura E, Rocha M, Tolentino H, Barbosa A, Craievich A & Torriani I (1997) The small-angle X-ray scattering beamline of the Brazilian synchrotron light laboratory. *J Appl Crystallogr* **30**, 880–883.
57 Hammersley AP, Svensson SO, Hanfland M, Fitch AN & Hausermann D (1996) Two-dimensional detector software: from real detector to idealised image or two-theta scan. *High Press Res* **14**, 235–248.
58 Konarev PV, Petoukhov MV, Volkov VV & Svergun DI (2006) ATSAS 2.1, a program package for small-angle scattering data analysis. *J Appl Crystallogr* **39**, 277–286.
59 Doniach S (2001) Changes in biomolecular conformation seen by small angle X-ray scattering. *Chem Rev* **101**, 1763–1778.
60 Franke D & Svergun DI (2009) DAMMIF, a program for rapid ab-initio shape determination in small-angle scattering. *J Appl Crystallogr* **42**, 342–346.
61 Volkov VV & Svergun DI (2003) Uniqueness of *ab initio* shape determination in small-angle scattering. *J Appl Crystallogr* **36**, 860–864.
62 Roy A, Kucukural A & Zhang Y (2010) I-TASSER: a unified platform for automated protein structure and function prediction. *Nat Protoc* **5**, 725–738.
63 Petoukhov MV & Svergun DI (2005) Global rigid body modeling of macromolecular

complexes against small-angle scattering data. *Biophys J* **89**, 1237–1250.
64 Svergun D, Barberato C & Koch MHJ (1995) CRYSOL a program to evaluate X-ray solution scattering of biological macromolecules from atomic coordinates. *J Appl Crystallogr* **28**, 768–773.
65 Kozin MB & Svergun DI (2001) Automated matching of high- and low-resolution structural models. *J Appl Crystallogr* **34**, 33–41.

Supporting information

The following supplementary material is available:
Fig. S1. CLUSTALW2 alignment of DsbC sequences from *X. fastidiosa* strain 9a5c (XfDsbC), *X. campestris* pv. *campestris* (XcDsbC), *E. chrysanthemi* (ErcDsbC) and *E. coli* (EcDsbC).
Fig. S2. The inverted $XfDsbC_{Red}$ dimer.
Fig. S3. Possible tetrameric assemblies of (A) EcDsbC (PDB code: 1EEJ) and (B) HiDsbC (PDB code: 1TDJ).

This supplementary material can be found in the online version of this article.

Please note: As a service to our authors and readers, this journal provides supporting information supplied by the authors. Such materials are peer-reviewed and may be reorganized for online delivery, but are not copy-edited or typeset. Technical support issues arising from supporting information (other than missing files) should be addressed to the authors.